Phase locking of multiple optical fiber channels for a slow-light-enabled laser radar system

Joseph E. Vornehm,[1,*] Aaron Schweinsberg,[1] Zhimin Shi,[1,2]
Daniel J. Gauthier,[3] and Robert W. Boyd[1,4]

[1] *Institute of Optics, University of Rochester, Rochester, New York 14627, USA*
[2] *Department of Physics, University of South Florida, 4202 East Fowler Ave, Tampa, FL 33620, USA*
[3] *Department of Physics, Duke University, P.O. Box 90305, Durham, North Carolina 27708, USA*
[4] *Department of Physics and School of Electrical Engineering and Computer Science, University of Ottawa, Ottawa, Ontario K1N 6N5, Canada*

[*]*vornehm@optics.rochester.edu*

Abstract: Phase control is crucial to the operation of coherent beam combining systems, whether for laser radar or high-power beam combining. We have recently demonstrated a design for a multi-aperture, coherently combined, synchronized- and phased-array slow light laser radar (SLIDAR) that is capable of scanning in two dimensions with dynamic group delay compensation. Here we describe in detail the optical phase locking system used in the design. The phase locking system achieves an estimated Strehl ratio of 0.8, and signals from multiple emitting apertures are phase locked simultaneously to within $\pi/5$ radians (1/10 wave) after propagation through 2.2 km of single-mode fiber per channel. Phase locking performance is maintained even as two independent slow light mechanisms are utilized simultaneously.

References and links

1. C. D. Nabors, "Effects of phase errors on coherent emitter arrays," Appl. Opt. **33**, 2284–2289 (1994).
2. S. J. Augst, T. Y. Fan, and A. Sanchez, "Coherent beam combining and phase noise measurements of ytterbium fiber amplifiers," Opt. Lett. **29**, 474–476 (2004).
3. T. Y. Fan, "Laser beam combining for high-power, high-radiance sources," IEEE J. Sel. Top. Quantum Electron. **11**, 567–577 (2005).
4. N. J. Miller, M. P. Dierking, and B. D. Duncan, "Optical sparse aperture imaging," Appl. Opt. **46**, 5933–5943 (2007).
5. W. Liang, N. Satyan, F. Aflatouni, A. Yariv, A. Kewitsch, G. Rakuljic, and H. Hashemi, "Coherent beam combining with multilevel optical phase-locked loops," J. Opt. Soc. Am. B **24**, 2930–2939 (2007).
6. W. Liang, A. Yariv, A. Kewitsch, and G. Rakuljic, "Coherent combining of the output of two semiconductor lasers using optical phase-lock loops," Opt. Lett. **32**, 370–372 (2007).
7. P. F. McManamon, "Review of ladar: A historic, yet emerging, sensor technology with rich phenomenology," Opt. Eng. **51**, 060901 (2012).
8. A. Schweinsberg, Z. Shi, J. E. Vornehm, and R. W. Boyd, "Demonstration of a slow-light laser radar," Opt. Express **19**, 15760–15769 (2011).
9. A. Schweinsberg, Z. Shi, J. E. Vornehm, and R. W. Boyd, "A slow-light laser radar system with two-dimensional scanning," Opt. Lett. **37**, 329–331 (2012).

10. Z. Shi, A. Schweinsberg, J. E. Vornehm, and R. W. Boyd, "A slow-light laser radar (SLIDAR)," Opt. Photon. News **23**, 51–51 (2012).
11. L. V. Hau, S. E. Harris, Z. Dutton, and C. H. Behroozi, "Light speed reduction to 17 metres per second in an ultracold atomic gas," Nature (London) **397**, 594–598 (1999).
12. M. S. Bigelow, N. N. Lepeshkin, and R. W. Boyd, "Superluminal and slow light propagation in a room-temperature solid," Science **301**, 200–202 (2003).
13. M. González Herráez, K. Y. Song, and L. Thévenaz, "Arbitrary-bandwidth Brillouin slow light in optical fibers," Opt. Express **14**, 1395–1400 (2006).
14. B. Zhang, L. Zhang, L.-S. Yan, I. Fazal, J. Yang, and A. E. Willner, "Continuously-tunable, bit-rate variable OTDM using broadband SBS slow-light delay line," Opt. Express **15**, 8317–8322 (2007).
15. F. Öhman, K. Yvind, and J. Mørk, "Slow light in a semiconductor waveguide for true-time delay applications in microwave photonics," IEEE Photon. Technol. Lett. **19**, 1145–1147 (2007).
16. R. M. Camacho, C. J. Broadbent, I. Ali-Khan, and J. C. Howell, "All-optical delay of images using slow light," Phys. Rev. Lett. **98**, 043902 (2007).
17. Y. Okawachi, R. Salem, and A. L. Gaeta, "Continuous tunable delays at 10-Gb/s data rates using self-phase modulation and dispersion," J. Lightwave Technol. **25**, 3710–3715 (2007).
18. Z. Zhu, A. M. C. Dawes, D. J. Gauthier, L. Zhang, and A. E. Willner, "Broadband SBS slow light in an optical fiber," J. Lightwave Technol. **25**, 201–206 (2007).
19. Z. Shi, A. Schweinsberg, J. E. Vornehm Jr., M. A. Martínez Gámez, and R. W. Boyd, "Low distortion, continuously tunable, positive and negative time delays by slow and fast light using stimulated Brillouin scattering," Phys. Lett. A **374**, 4071–4074 (2010).
20. S. J. Augst, J. K. Ranka, T. Y. Fan, and A. Sanchez, "Beam combining of ytterbium fiber amplifiers (Invited)," J. Opt. Soc. Am. B **24**, 1707–1715 (2007).
21. P. Zhou, Z. Liu, X. Wang, Y. Ma, H. Ma, X. Xu, and S. Guo, "Coherent beam combining of fiber amplifiers using stochastic parallel gradient descent algorithm and its application," IEEE J. Sel. Top. Quantum Electron. **15**, 248–256 (2009).
22. A. M. Marino and C. R. Stroud, "Phase-locked laser system for use in atomic coherence experiments," Rev. Sci. Instrum. **79**, 013104 (2008).
23. T. M. Shay and V. Benham, "First experimental demonstration of phase locking of optical fiber arrays by RF phase modulation," Proc. SPIE **5550**, 313–319 (2004).
24. T. M. Shay, V. Benham, J. T. Baker, B. Ward, A. D. Sanchez, M. A. Culpepper, D. Pilkington, J. Spring, D. J. Nelson, and C. A. Lu, "First experimental demonstration of self-synchronous phase locking of an optical array," Opt. Express **14**, 12015–12021 (2006).
25. M. A. Vorontsov, G. W. Carhart, and J. C. Ricklin, "Adaptive phase-distortion correction based on parallel gradient-descent optimization," Opt. Lett. **22**, 907–909 (1997).
26. L. Liu and M. A. Vorontsov, "Phase-locking of tiled fiber array using SPGD feedback controller," Proc. SPIE **5895**, 58950P (2005).
27. X. Wang, P. Zhou, Y. Ma, J. Leng, X. Xu, and Z. Liu, "Active phasing a nine-element 1.14 kW all-fiber two-tone MOPA array using SPGD algorithm," Opt. Lett. **36**, 3121–3123 (2011).

1. Introduction

Optical systems that make use of coherent beam combining, including multi-aperture laser radar systems such as ours, depend critically upon having coherent, properly phased signals from each emitter to achieve constructive interference at the target [1–7]. In a multi-aperture laser radar, optical fields from multiple small emitters propagate to a target in the far field, where they overlap and combine coherently, allowing agile beam steering. The interference pattern produced by these fields has a finer transverse resolution (and higher peak intensity) than that of the individual emitters; a well-designed array can achieve a transverse far-field resolution approaching that of a single large emitter of the same size as the entire array. However, proper coherence and phase relations must be maintained among all emitters. Otherwise, the far-field transverse resolution and intensity are degraded, losing the advantage of multiple emitters.

Slow light can enhance the transverse and longitudinal resolution of a short-pulse, multi-aperture, coherently combined laser radar system, as we have recently demonstrated with our SLIDAR (slow-light laser radar) system [8–10]. Slow light, or light that travels at extremely slow yet controllable group velocities, has emerged not only as an intriguing area of fundamental science but also with promise as an important enabling technology for diverse applications,

especially in optical fibers [11–19]. The use of tunable slow-light delay lines in a multi-aperture short-pulse laser radar overcomes the fundamental limitation of group delay mismatch during wide-angle beam steering. In our SLIDAR system, two independent slow light methods provide tunable true time delay to allow steering in two transverse dimensions.

We present here the phase locking techniques used in SLIDAR. The phase locking system satisfies the need for a simple, inexpensive, yet reasonably effective phase control system to allow the proper phasing of each emitter. An electro-optic phase modulator (EOM) serves as the phase actuator, and each emitter's output signal is monitored by a single-quadrature phase detector in a heterodyne configuration. A proportional-integral analog control circuit maintains phase lock to within $\pi/5$ radians RMS. A novel fast $2n\pi$ phase snapback circuit overcomes the problem of finite phase actuation range.

2. Theory

For a fixed emitter configuration and constant power, the intensity of the received optical signal is directly proportional to the Strehl ratio, or the ratio of the actual peak combined intensity to the theoretical maximum in the absence of phase noise [1, 2]. A hypothetical phase locking system with infinite bandwidth (instantaneous response) would have no residual phase error, and its Strehl ratio would be 1. Of course, all causal phase locking systems will have some finite residual phase error, so the actual Strehl ratio will be somewhat degraded. In the total absence of phase lock, the Strehl ratio drops to $1/N$ for an N-emitter system, and the transverse far-field resolution is degraded to the resolution of a single emitter, negating nearly all of the benefits of using a multi-aperture system. The importance of phase lock to the proper operation of a coherently-combined system cannot be overstated.

The Strehl ratio can be estimated based on the measured phase noise of the system. Specifically, we model the phase errors of our system and find their influence on the Strehl ratio. In doing so, we follow the derivation given by Nabors [1] for the grating Strehl ratio (we neglect the impact of the emitter field profile).

Our system has two main contributions to the phase error, both of which can be seen in Fig. 1. The first is the residual phase error, or the small amount of phase noise that remains after correction by the phase control system. The second is the error due to $2n\pi$ phase snapback events. Both are random processes, and their statistics depend strongly on environmental conditions, such as temperature fluctuations and vibrations. To gain some insight into their respective effects, we make some simplifying assumptions. First, we take the residual phase noise to have a Gaussian distribution with zero mean and variance σ^2, and we assume that the phase noise at one moment is independent of the phase noise at a different time (meaning the residual phase noise is a stationary process). Second, we model the snapback process as a linear $2n\pi$ phase ramp of duration τ that occurs at random times, with the snapback times having a Poissonian distribution with rate r. Finally, we assume each emitter's noise processes are statistically independent of those of the other emitters.

2.1. The effect of residual phase error

Assume that each of N emitters have identical field profiles $u_0(x,y)$, each with identical amplitude, relative position (x_j, y_j), and random phase ϕ_j:

$$u(x,y) = u_0(x,y) * \sum_{j=1}^{N} \delta(x-x_j, y-y_j)\exp(i\phi_j) = u_0(x,y) * g(x,y), \qquad (1)$$

where the asterisk indicates convolution, and $\delta(x,y) = \delta(x)\delta(y)$ is a two-dimensional Dirac delta. The function $g(x,y)$ is called the near-field grating function. In the Fraunhofer regime,
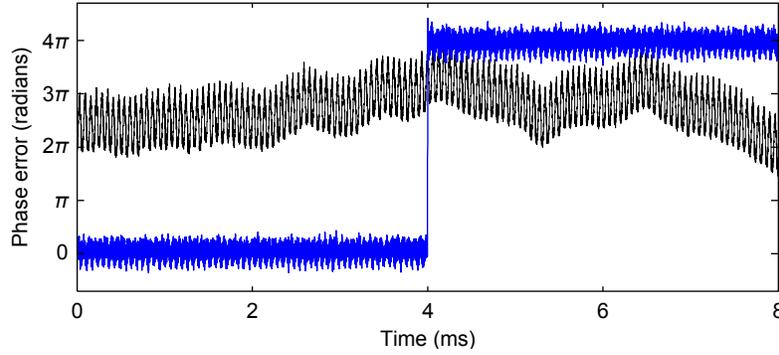
Fig. 1. An 8 ms sample of raw, uncorrected phase noise (black line) and phase error after correction by the phase control system (blue line). The phase error consists of two parts: the zero-mean residual phase error and the 4π snapback event that occurs at 4 ms. (Only the phase error modulo 2π affects system performance.)

the far field $U(f_x, f_y) = U_0(f_x, f_y)G(f_x, f_y)$, where

$$U_0(f_x, f_y) = \iint u_0(x, y) \exp[i2\pi(f_x x + f_y y)] \, dx \, dy \tag{2}$$

and

$$G(f_x, f_y) = \sum_{j=1}^{N} \exp[i2\pi(f_x x_j + f_y y_j) + i\phi_j]. \tag{3}$$

Here, $U_0(f_x, f_y)$ is the far-field pattern produced by a single emitter, and $G(f_x, f_y)$ is the far-field grating pattern. The far-field intensity can then be expressed as

$$I(f_x, f_y) = |U(f_x, f_y)|^2 = |U_0(f_x, f_y)|^2 |G(f_x, f_y)|^2. \tag{4}$$

Assuming the far-field intensity has a peak at $I(0,0)$, we define the Strehl ratio as

$$S = \frac{\langle I(0,0) \rangle}{I_{\max}(0,0)} = \frac{|U_0(0,0)|^2 \langle |G(0,0)|^2 \rangle}{|U_0(0,0)|^2 [\max|G(0,0)|^2]} = \frac{\langle |G(0,0)|^2 \rangle}{\max|G(0,0)|^2}, \tag{5}$$

where angle brackets indicate the expected value. We evaluate $|G(0,0)|^2$ as

$$G(0,0)G^*(0,0) = \left[\sum_{j=1}^{N} \exp(i\phi_j)\right]\left[\sum_{j=1}^{N} \exp(-i\phi_j)\right] = \sum_{j=1}^{N} \left[1 + 2\sum_{k=j+1}^{N} \cos(\phi_j - \phi_k)\right], \tag{6}$$

which reaches its maximum value of N^2 when all of the ϕ_j are equal. Hence, $\max|G(0,0)|^2 = N^2$, and

$$S = \frac{1}{N^2} \langle |G(0,0)|^2 \rangle = \frac{1}{N^2} \sum_{j=1}^{N} \left[1 + 2\sum_{k=j+1}^{N} \langle \cos(\phi_j - \phi_k) \rangle\right]. \tag{7}$$

Considering only the effects of the zero-mean Gaussian residual phase error, the innermost term of Eq. (7) becomes

$$\langle \cos(\phi_j - \phi_k) \rangle = \iint \frac{1}{2\pi\sigma^2} \exp\left(\frac{-\phi_j^2 - \phi_k^2}{2\sigma^2}\right) \cos(\phi_j - \phi_k) \, d\phi_j \, d\phi_k = \exp(-\sigma^2). \tag{8}$$

Then

$$S = \frac{1}{N^2} \sum_{j=1}^{N} \left[1 + 2 \sum_{k=j+1}^{N} \exp(-\sigma^2) \right] = \frac{1}{N} + \frac{N-1}{N} \exp(-\sigma^2). \tag{9}$$

(This expression matches the expression given by Nabors for the case of uncorrelated phase errors [1].) We see this expression is the sum of incoherent and coherent contributions. In the limit of complete incoherence among the emitters (large σ), the Strehl ratio is $1/N$, as would be expected for an incoherent sum. In the case of perfect coherence and perfect phase synchronization ($\sigma = 0$), the Strehl ratio becomes 1.

2.2. The effect of snapbacks

A snapback event happens when the phase actuator (an electro-optic modulator in our experiment) reaches the end of its range and is quickly shifted, or "snaps back," by $2n\pi$ in order to maintain phase lock. We model this as a linear phase ramp, shifting the phase by $2n\pi$ over an interval τ. We define the phase error of each emitter as the sum of two stochastic processes

$$\phi_j(t) = \phi_{R,j}(t) + \phi_{S,j}(t), \tag{10}$$

where $\phi_{R,j}(t)$ is the (Gaussian) residual phase error of emitter j, as described above. Here, $\phi_{S,j}(t)$ represents the snapback process in emitter j as follows: If a snapback event occurs at time t_0, then $\phi_{S,j}(t) = 2n\pi(t - t_0)/\tau$ for $t_0 \leq t < t_0 + \tau$, and τ is the duration of a snapback phase ramp. For times at which no snapback occurs, $\phi_{S,j}(t) = 0$. Snapback events occur at random times, following a Poisson process; that is, they occur with an average rate r (measured in events per unit time), and the probability that m snapback events occur in an interval T is a Poisson random variable with dimensionless parameter rT

$$P(m; T) = \exp(-rT) \frac{(rT)^m}{m!}. \tag{11}$$

Note that the average rate r of snapback events does not change with time, although the number of snapbacks in any interval depends on the length of the interval (and will be rT on average).

The snapback duty cycle, or average fraction of time spent in a snapback process, is equal to $r\tau$. Intuitively, the snapback duty cycle must be kept low [20], so we require that $r\tau \ll 1$. We make the further simplifying assumption that snapback events never overlap in time, either on the same emitter or on different emitters. (It can be shown that this assumption is slightly pessimistic, but in the limit of low snapback duty cycle it is accurate.)

To understand how snapback events impact system performance, we must consider the time-averaged Strehl ratio. We define the time average of the Strehl ratio over an interval from from t_0 to t_1 as

$$\langle S(t) \rangle_{t_0, t_1} = \frac{1}{t_1 - t_0} \int_{t_0}^{t_1} S(t) \, dt. \tag{12}$$

By substituting the definition of the Strehl ratio from Eq. (7), we find

$$\langle S(t) \rangle_{t_0, t_1} = \frac{1}{N^2} \left\langle \langle |G(0,0;t)|^2 \rangle \right\rangle_{t_0, t_1} = \left\langle \left\langle \sum_{j=1}^{N} \left[1 + 2 \sum_{k=j+1}^{N} \cos(\phi_j(t) - \phi_k(t)) \right] \right\rangle \right\rangle_{t_0, t_1}$$

$$= \frac{1}{N^2} \sum_{j=1}^{N} \left\{ 1 + 2 \sum_{k=j+1}^{N} \left\langle \langle \cos[\phi_{R,j}(t) - \phi_{R,k}(t) + \phi_{S,j}(t) - \phi_{S,k}(t)] \rangle \right\rangle_{t_0, t_1} \right\}. \tag{13}$$

The subscripted angle brackets indicate a time average, while angle brackets without a subscript indicate a statistical average.

Let us consider the impact of a single snapback event on the inner expression in Eq. (13). We assume that emitter j experiences a $2n\pi$ snapback event of duration τ, such that $\phi_{S,j}(t) = 2n\pi(t-t_0)/\tau$ over the interval t_0 to $t_0+\tau$, while emitter k experiences no snapback event; then

$$\langle\langle\cos[\phi_{R,j}(t) - \phi_{R,k}(t) + 2n\pi(t-t_0)/\tau]\rangle\rangle_{t_0,t_0+\tau}$$

$$= \left\langle \iint \frac{1}{2\pi\sigma^2}\exp\left(\frac{-\phi_j^2 - \phi_k^2}{2\sigma^2}\right)\cos[\phi_j - \phi_k + 2n\pi(t-t_0)/\tau]\,d\phi_j\,d\phi_k\right\rangle_{t_0,t_0+\tau}$$

$$= \langle\exp(-\sigma^2)\cos[2n\pi(t-t_0)/\tau]\rangle_{t_0,t_0+\tau} = 0. \quad (14)$$

In other words, an emitter undergoing a snapback makes no coherent contribution to the time-averaged Strehl ratio during the time that the snapback is occurring. Conversely, if there is no snapback occurring, the coherent contribution to the time-averaged Strehl ratio is as before,

$$\langle\langle\cos[\phi_{R,j}(t) - \phi_{R,k}(t)]\rangle\rangle_{t_0,t_0+\tau} = \langle\exp(-\sigma^2)\rangle_{t_0,t_0+\tau} = \exp(-\sigma^2). \quad (15)$$

One can think of each snapback (of duration τ) occurring in an interval T as reducing the coherent contribution to the time-averaged Strehl ratio by an amount τ/T. If m snapback events happen during the interval T, the coherent contribution will be reduced by $m\tau/T$. (For simplicity, we neglect the possibility of edge cases, or snapbacks that happen very near the end of the interval.) The probability that m snapbacks occur in an interval T is given by Eq. (11), so we can compute the expected value of the time-averaged Strehl ratio over an interval T with a given average snapback rate r and residual phase noise variance σ^2

$$\langle S(t)\rangle_{t_0,t_0+T} = \frac{1}{N^2}\langle\langle|G(0,0;t)|^2\rangle\rangle_{t_0,t_0+T}$$

$$= \frac{1}{N^2}\sum_{m=0}^{\infty}P(m;T)\sum_{j=1}^{N}\left[1 + 2\sum_{k=j+1}^{N}\left(1 - \frac{m\tau}{T}\right)\exp(-\sigma^2)\right]$$

$$= \frac{1}{N} + \frac{N-1}{N}(1-r\tau)\exp(-\sigma^2). \quad (16)$$

By comparing Eq. (16) to Eq. (9), we can see that the effect of snapbacks is to reduce the coherent contribution to the time-averaged Strehl ratio by the factor $(1-r\tau)$.

As one might expect, the result given in Eq. (16) does not depend on t_0 or T, only on the snapback duty cycle $r\tau$. To maximize the Strehl ratio, we must minimize both the rate r at which snapback events occur and their duration τ (or minimize the snapback duty cycle, coinciding with our assumption $r\tau \ll 1$). Interestingly, n, the number of 2π phase cycles in each snapback event, influences the time-averaged Strehl ratio only indirectly. Increasing n may decrease r, since larger jumps may mean fewer snapbacks, but it will generally also increase τ, since a larger phase change will take longer to complete. The balance of these effects depends on the actual parameters of the phase control system and the statistics of the (uncorrected) phase noise. Of course, maximizing the Strehl ratio also means minimizing σ.

It bears repeating that the phase noise in a given system is highly dependent on several environmental variables, particularly temperature and vibration. The assumption of a stationary Gaussian noise process is inaccurate for many models of phase noise, which often have an RMS value that increases with time (and are therefore non-stationary processes). The rate at which snapbacks occur depends highly on the phase noise in the system and may well be non-Poissonian. Nevertheless, the above derivation gives a useful picture of how the residual phase error and the snapback process affect the Strehl ratio, and in particular that the snapback process does not significantly affect the Strehl ratio if the duty cycle is kept low.

3. Experimental apparatus

3.1. Optical system

The layout of the optical system is shown in Fig. 2. A fiber-coupled tunable laser generates about 1 mW of continuous-wave (cw) light near 1550 nm. The laser feeds both a phase reference arm and a pulse carver followed by several signal channels (three channels in our system). The pulse carver consists of an intensity modulator driven by an arbitrary function generator, as well as an erbium-doped fiber amplifier (EDFA) and fiber polarization controllers. The reference arm is frequency-shifted by 55 MHz using an acousto-optic modulator (AOM), and the frequency-shifted reference is used for heterodyne detection to monitor the phase of each signal channel and maintain phase lock. The local oscillator (LO) used by the AOM to frequency-shift the reference is also used by the phase locking electronics in each channel.
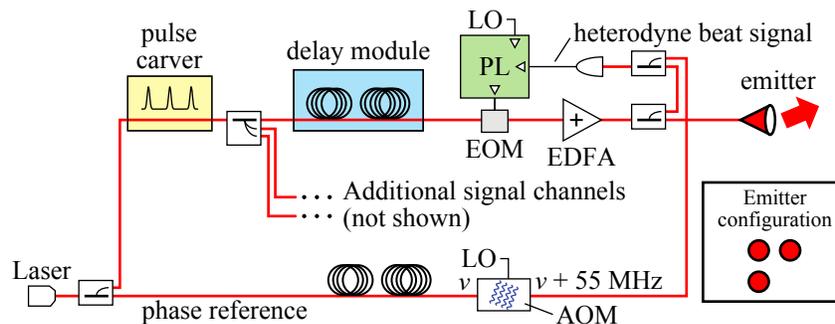

Fig. 2. Schematic diagram of the optical system (see text for details). A fraction of each channel's output signal is heterodyned with a frequency-shifted reference to monitor the phase. Phase locking electronics (PL) feed back to an electro-optic modulator (EOM) to control the phase. The local oscillator (LO) used to frequency-shift the phase reference is also used by the phase locking electronics. Inset: Emitter configuration, as seen looking into the emitters.

Each signal channel contains a slow-light delay module consisting of 2.2-km length of single-mode fiber (SMF), either dispersion-compensating fiber (DCF) or dispersion-shifted fiber (DSF). The ratio of DCF to DSF in each module creates a relative dispersive delay between each signal arm [17]. One of the delay modules also contains a counter-propagating pump (not shown in Fig. 2) to induce stimulated Brillouin scattering (SBS) slow light [18, 19]. By controlling the wavelength of the optical field and the pump power of the SBS module, one can achieve independent group delay compensation in two orthogonal transverse dimensions. Details of the group delay modules have been reported previously [8, 9].

After the delay module, each signal channel contains an EOM to compensate for phase errors, an EDFA to maintain constant output amplitude (particularly important to compensate for the variable gain of SBS slow light), and an emitter (a fiber output coupler), as well as a splitter to tap off a fraction of the output signal, a heterodyne detection setup, and phase locking electronics, described below. All channels are phase locked to the same reference. Our system uses three signal channels, with the three emitters in an L-shaped arrangement that allows two-dimensional steering (shown in the inset of Fig. 2). Note that the short length of fiber in each channel between the last splitter and the emitter cannot be monitored for phase noise; this uncompensated fiber length is kept as short as possible to minimize the additional phase noise it contributes to the system.

The pulse carver creates 6.5 ns pulses (FWHM) on a cw background of about 30% of the peak power. The pulse duration is shorter than the response time of the phase control electronics, so

the phase control circuit does not "see" the pulse. Only the cw background is used by the phase control electronics.

3.2. Electronics

A block diagram of the phase control electronics is shown in Fig. 3. In essence, a phase-sensitive detection is performed on each signal channel's heterodyne signal, using a phase-shifted version of the 55 MHz local oscillator as a reference; the result is a voltage proportional to the phase difference between the heterodyne and the LO, which is passed to a proportional-integral (P-I) controller. The phase-shifting of the LO allows each channel to be phased independently, allowing full control over the far-field pattern. The P-I controller consists of a loop filter with gain and a fast $2n\pi$-phase snapback circuit. It filters the error signal and drives the EOM. The design of the P-I controller is shown in Fig. 4. PSpice circuit simulations and laboratory measurements of the loop filter transfer function show the loop filter bandwidth to be about 2.3 MHz.
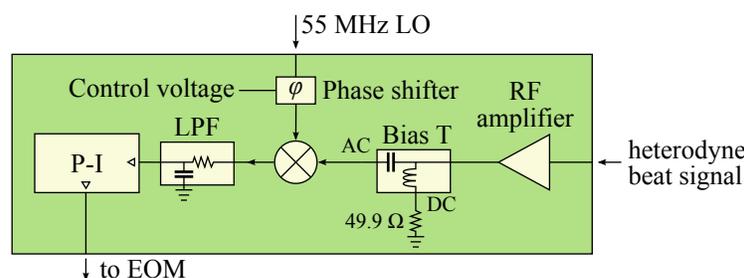

Fig. 3. Block diagram of the phase control electronics. The 55 MHz local oscillator (LO) is phase-shifted to allow independent, arbitrary phasing of each channel. The heterodyne signal is amplified, its DC bias is removed by the bias T, and it is mixed with the LO and then low-pass filtered (LPF) to perform a phase-sensitive detection of the heterodyne signal. The resulting signal is then fed to the proportional-integral (P-I) controller.

The phase error accumulates rapidly in the P-I controller, and the control signal to the EOM cannot exceed supply voltages of the loop filter. The half-wave voltage (V_π) of our EOM is nominally 4 V, and the loop filter uses ± 15 V supply voltages, giving a phase actuation range of somewhat over 6π (allowing some margin). To maintain phase lock over many cycles, a fast $2n\pi$-phase snapback circuit is implemented, which rapidly adds or subtracts $2n\pi$ radians from the phase error being tracked by the P-I controller whenever the controller's output voltage approaches a voltage supply level. In this way, the P-I controller is able to track an unbounded amount of phase error. These brief (about 1.2 μs) phase snapback events do not impact performance as long as the snapback duty cycle is kept low, as discussed in Section 2. The operation of the snapback circuit is as follows: When the loop filter's output V_{EOM} exceeds a certain threshold (nominally $3V_\pi$ or $+12$ V), an analog switch engages and strongly drives V_{EOM} toward negative voltages. Once V_{EOM} is below a second, lower threshold (nominally V_π or $+4$ V), the analog switch disengages, and the loop filter resumes tracking, having shifted its operating point by 2π radians of phase error. A corresponding process occurs for negative values of V_{EOM}. In practice the exact threshold voltages (as well as the resistor and capacitor values) are tuned empirically to account for several parameters such as the drive strength (maximum output current) of the analog switch and the response times of the switch and the loop filter, and the circuit is typically adjusted to provide a 4π phase snapback. (We verified experimentally that the op-amp never enters saturation because the switch is disengaged as soon as V_{EOM} crosses the appropriate threshold.)
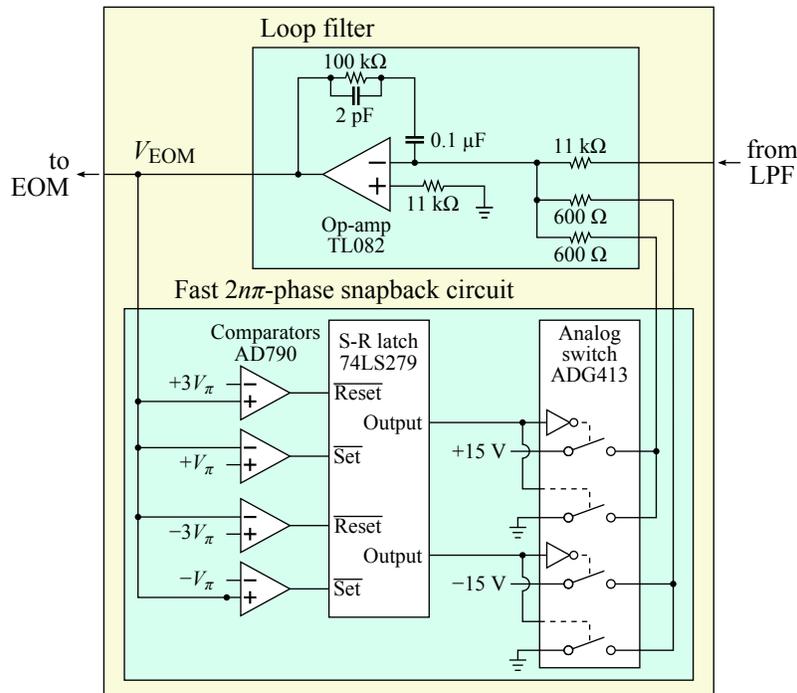
Fig. 4. Block diagram of the proportional-integral (P-I) controller, including the loop filter and the fast $2n\pi$-phase snapback circuit. The signal from the low-pass filter (LPF) in Fig. 3 is the primary input to an integrating op-amp that tracks the phase error and drives the EOM. When the op-amp output voltage V_{EOM} exceeds $\pm 3V_\pi$ (nominally ± 12 V), a set-reset (S-R) latch engages an analog switch that quickly drives V_{EOM} toward the opposite polarity; the switch disengages once V_{EOM} is within the range $\pm V_\pi$ (nominally ± 4 V). The process typically takes about 1.2 μs. In practice, the comparator bias voltages and the resistor and capacitor values are tuned for optimal snapback performance and are usually selected to provide a 4π snapback. (Some circuit elements are not shown, including buffering op-amps, diodes, and a power-on reset circuit.)

4. Results and discussion

Figure 5 shows the phase locking performance of the phase control system in a single SLIDAR channel containing 2.2 km of single-mode DSF, averaged over 20 seconds. Over this time window, the RMS residual phase error is approximately $\pi/5$ radians (1/10 wave). The theoretically-predicted Strehl ratio due to the RMS residual phase error, according to Eq. (16), is about 0.8, comparable to results obtained in several other optical phase locking systems [20,21].

Phase lock is maintained in the presence of both SBS slow light and dispersive slow light over the full range of operation. The varying SBS gain is compensated by the final EDFA in each signal channel, which ensures a constant heterodyne signal level. Some slight pulse shape distortion due to the SBS process is evidenced but does not affect the phase locking performance. Broadening of the SBS pump, a common technique in SBS slow light [18, 19], is found not to induce any differences in phase locking behavior. DCF, which is used only for dispersive slow light and not SBS slow light, sees the same phase locking performance as unpumped DSF; further, the performance does not vary with wavelength.
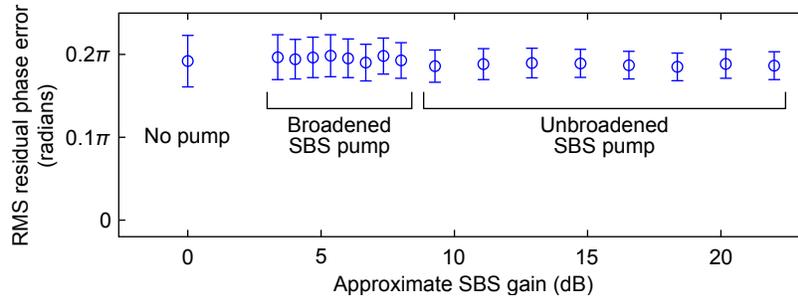
Fig. 5. RMS residual phase error vs. approximate SBS gain, showing about $\pi/5$ radians RMS residual phase error for all SBS gain values, with the SBS pump both broadened and unbroadened. In our system, the dispersion-compensating fiber used to achieve dispersive slow light performs similarly to the dispersion-shifted fiber used here to achieve SBS slow light, including under changes in wavelength.

The residual phase error was obtained by using an oscilloscope in a fast acquisition mode to measure the RMS jitter between the local oscillator and the heterodyne signal. Multiplying the RMS jitter (measured in picoseconds) by 2π times the LO frequency gives the RMS phase error. The measurements were taken while the phase lock was operating, and they include both optical and electronic contributions. The oscilloscope's fast acquisition mode allows repeated measurements of the RMS jitter over any desired duration, but at the expense of losing the time traces, which cannot be directly recorded. The residual phase error was observed not to change appreciably between acquisition times of 1 s and 20 s.

The uncorrected phase noise cannot be measured directly in our experiment, but adding the residual phase error and the applied phase shift due to the EOM gives an estimate of the phase noise. A sample trace of the phase noise obtained in this way was presented earlier, in Fig. 1. The applied phase shift is estimated from a time trace of the EOM control voltage (V_{EOM}). The residual phase error is computed by performing software heterodyne detection (mixing and low-pass filtering) on time traces of the local oscillator and the heterodyne signal. Because the time traces must be sampled at more than twice the LO frequency of 55 MHz, the oscilloscope buffer is limited to traces of 8 ms duration.

Figure 6 shows a real-time video of the far-field pattern with and without phase locking. In our laboratory environment, the primary sources of phase noise are believed to be temperature changes and vibration [20]. The phase error tends to drift continuously in one direction (either positive or negative), which we presume to be due to environmental temperature changes. Under these conditions, using a 4π snapback rather than 2π tends to reduce the rate of snapback events. The snapback rate r fluctuates, but the measured average is about two snapback events per second. A single snapback event takes 1.2 μs, so the snapback duty cycle $r\tau$ is about 2.4×10^{-6}. At this low level, the snapback process has a negligible effect on the Strehl ratio; even a duty cycle several orders of magnitude larger would not impact the Strehl ratio noticeably. In our system, the maximum achievable snapback size is 4π, limited by the drive strength of the analog switch, the response times of various components, and other factors, as discussed in Section 3.2. While a larger snapback size might further reduce the impact of the snapback cycles on the residual phase error (see Section 2.2), the present system provides adequate performance for the purposes of SLIDAR.

Other researchers have developed several quite versatile phase locking techniques, such as optical phase-locked loops (OPLL) [5, 6, 22] and LOCSET [23, 24]. However, our slow light system precludes the use of tuning the source laser wavelength, as in an OPLL, and requires
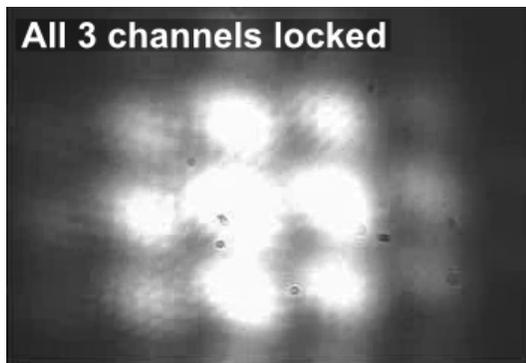
Fig. 6. (Media 1) A representative image from a real-time video showing the far-field pattern of the three-channel system, first with phase locking disabled and then with phase locking enabled (image taken when phase locking is enabled). When phase locking is disabled, the bright lobes in the far-field pattern shift rapidly in both transverse dimensions, since the points of constructive interference change with the emitter phases. When phase locking is enabled, the lobes lock into place, with a small but still visible amount of jitter.

that all signal channels operate at the same frequency, unlike LOCSET. Further, the phase locking system presented here does not require the complex and expensive signal processing electronics used by such feedback control methods as stochastic parallel gradient descent (SPGD) optimization [25–27]. (Of course, a fast $2n\pi$ snapback process can certainly be implemented in a digital signal processing system.)

5. Conclusion

We have demonstrated a simple, effective phase locking system using an electro-optic phase modulator and a feedback circuit with a fast $2n\pi$-phase snapback to allow unlimited phase actuation range. The system maintains phase lock among three channels of 2.2 km each of single-mode fiber while utilizing two different slow light techniques, with the RMS residual phase error around $\pi/5$ radians (Strehl ratio around 0.8) The phase locking approach is scalable to many more channels, as each channel is independently locked to an optical reference. The approach presented here should also be applicable to coherent beam combining, where fiber lengths are typically limited to tens of meters.

Acknowledgments